ELEVENTH EUROPEAN ROTORCRAFT FORUM

Paper No. 3

THEORETICAL AND EXPERIMENTAL CORRELATION OF LOW-SPEED MODEL HELICOPTER BLADE SLAP

Daniel Chin-Leung Chan
Project Engineer
General Motors Corporation

James E. Hubbard, Jr.
Assistant Professor of Mechanical Engineering

Massachusetts Institute of Technology
Cambridge, MA 02139
U.S.A.

Eleventh European Rotorcraft Forum
10-13 September, 1985
London, England

THEORETICAL AND EXPERIMENTAL CORRELATION OF LOW-SPEED MODEL HELICOPTER BLADE SLAP

Daniel Chin-Leung Chan
Project Engineer
General Motors Corporation

James E. Hubbard, Jr.
Assistant Professor of Mechanical Engineering
Massachusetts Institute of Technology
Cambridge, MA 02139
U.S.A.

ABSTRACT

An instrumented model rotor blade equipped with differential pressure transducers and hot film sensors has been tested in the M.I.T. 1.52 m x 2.3 m (5 x 7.5 ft) anechoic wind tunnel to investigate the blade slap caused by blade-vortex interaction at tip Mach number less than 0.2. For the operating conditions tested, blade slap is caused by the vortex induced unsteady pressure fluctuations at the leading edge of a rotor blade during the blade-vortex interaction. The intensity of the resulting noise has a very profound dependancy on the interaction angle and/or the separation distance between the blade and the vortex filament increases. The measured acoustic signals have been compared with the predictions provided by the Widnall and Wolf Theory. Good correlations have been shown for the blade-vortex interactions occuring in a region outside the vortex core. The skew interaction effect is not modelled by the theory and is the cause of poor correlation with the experiment.

INTRODUCTION

Rotor noise can be classified into two main catagories: 1) Broadband noise and 2) Harmonic noise. Broadband noise is caused by unsteady load fluctuations due to inflow turbulence and a turbulent boundary layer passing over the trailing edge, as well as vortex shedding. Harmonic noise can also be divided into two groups: rotational noise and impulsive noise. Rotational noise is related to the mean lift and drag forces produced by the helicopter blade during flight manuevers. Impulsive noise, or blade slap, is the most annoying noise and has been the focus of attention for many

helicopter researchers in aerospace companies, universities and government laboratories. Historically, four mechanisms have been postulated for the cause of blade slap: 1) Unsteady pressure fluctuation due to blade vortex interaction (BVI). 2) Separation and reattachment of the boundary layer due to intermittent stall. 3) Local formation of shock waves. 4) Blade thickness.

There are several existing theories which attempt to predict the aerodynamic noise generated by the rotor during BVI. Farassat[1] applies the Ffowcs Williams-Hawkings equation to calculate near and far field acoustic signatures generated by a rotor. There are no restrictions on blade shape, tip Mach number or forward motion of the blades and the acoustic sources may be non-compact as well as compact. This theory, however, requires a description of body geometry, time history of motion and detailed surface pressure distribution on the blades as input parameters, therefore, rather involved and costly experiments are required. Nakamura[2] followed a similar approach and used the pressure measurements obtained by one hundred and forty pressure transducers flush mounted on a full scale helicopter blade as inputs to the acoustic model. He was unable to show good correlation and his theory underpredicted the peak-to-peak sound pressure to nearly one-fifth of the measured value. He concluded that the discrepancy was due to insufficient pressure measurements. Widnall and Wolf[3] exploit the assumptions which one can make in the case of low speed blade slap to yield a formulation which relates the rotor operation parameters to the acoustic far field. In light of its simplicity, this theory seems quite attractive, particularly in the case of low speed descent when BVI is most likely to occur.

The objective of this research is to investigate the operating conditions under which the assumptions made in the Widnall and Wolf model are valid. Using a limited number of miniature pressure transducers on a scale model helicopter rotor blade, the load distribution near the tip is estimated. This is then used as input to the Widnall and Wolf model to determine the structure of the trailing vortex. The geometry of the blade vortex interaction is determined through smoke visualization techniques developed by Fontana and Hubbard[4]. The vortex is modelled as a series of sinusoidal gusts. The unsteady load on the blade resulting from the blade/gusts interaction is then modelled as a distribution of acoustic dipoles. The predicted sound pressure level is compared with the experimentally obtained far field acoustic signature and recorded simultaneously with blade surface pressure measurements. Hot-film gauges are also used to determine the nature of the attached flow during the experiments.

EXPERIMENTAL EQUIPMENT

This study was performed in the M.I.T. anechoic wind tunnel. It is of closed circuit type, and can achieve a maximum free stream velocity of 34 m/sec. The tunnel has a 1.52 m x 2.4 m open jet test section. Polyurethane open-cell foam was used as an acoustic treatment for the floor during the tests. Cremer blocks and porous cloth bags filled with fiberglass blocks were used to cover both the ceiling and wall surfaces. This acoustic treatment provided a far field cutoff frequency of 160 Hz. The model rotor has a radius of 0.6 m. The rotor blades were made of balsa wood with a fiberglass skin. They were mounted on a hub which floats on a pair of four spoke supports. Collective pitch and shaft tilt angle can be adjusted manually. There is no provision for cyclic pitch. A two-bladed rotor with zero tilt angle was employed for this experiment. In addition, the rotor was operated in an inverted configuration to reduce the interference of the tunnel floor on the rotor wake and to allow easy access for acoustic measurements which were collected using a half-inch Bruel and Kjaer condenser microphone. The microphone was located directly above the rotor to measure the peak sound pressure level which occurs at this location[5]. In conjunction with the microphone, a B-Weighting network was used to measure the sound pressure level and to record the time history of the acoustic signature to minimize the interference due to the ambient noise and activities outside the anechoic wind tunnel. The effects of the filter on the pulse shape were studied and reported by Chan[6]. Figure 1 depicts the layout of the wind tunnel and the rotor configuration. The rotor blades have a NACA 0012 airfoil section with a 50.8 mm chord and a negative twist of 8 degrees. Seven semi-conductor type differential pressure transducers were flush mounted in the outer 25 percent of the tip region of the blade to measure the dynamic loading. The Widnall and Wolf model has a very profound dependance on the slope of the spanwise load distribution at the tip, therefore, three pressure transducers were located at 18.75, 50 and 85 percent chord positions at 99 percent span to obtain a better approximation of the slope. Three additional pressure transducers were located along the same chordwise positions at the 76 percent span where the maximum circulation is estimated to occur. Figure 2 shows the installation of these pressure transducers. The pressure transducers located at the 76 percent span were tested in the M.I.T. 2.5 cm x 2.5 cm low turbulence wind tunnel prior to the rotor test to verify the calibration data and to quantify the error in pressure measurements. The results were compared with the predictions provided by McFarland's panel program[7]. The measurements correlate

well with the theory at angles of attack less than 10 degrees. Six high bandwidth hot-film gauges were also flush mounted on the suction side of the blade to investigate the boundary layer characteristic during blade/vortex interaction. A schematic of the instrumented blade is shown in Figure 3. The output from all the sensors and microphone were recorded simultaneously on a 14-channel Racal Type 14D FM Instrumentation Recorder. The Nicolet 660B Dual Channel FFT Analyzer provided the provision for the on-line examination of the power spectra of the outputs. Figure 4 illustrates the organization of the data acquisition system. The stationarity of the data was also investigated. All the impulsive changes due to BVI recorded in this experiment were found to be stationary[6].

THEORETICAL MODEL

The variation of the loading along the span causes the shedding of a vortex sheet behind the rotor blade. This vortex sheet eventually rolls up and moves inboard to form a concentrated vortex filament. Betz applies the laws of conservation of momentum in potential flow to relate the structure of the vortex to the spanwise load distribution on a wing. The three conservation relations are: 1) Circulation is conserved. 2) Centroid of vorticity remains at a fixed spanwise location. 3) Second moment of vorticity is conserved. Betz's theory, however, does not predict the structure of the inner core region where the viscosity is dominant and is roughly a rigid body rotational flow. This is, in fact, the weakest link of the theory and may fail to provide good predictions if the interaction occurs in the vicinity of the vortex core. Donaldson et. al.[10] suggest that only the vorticity bounded between the helicopter blade tip and the position of maximum spanwise circulation rolls up into a tip vortex. Rossow[11] further simplifies Betz's model and postulates two equations to relate the circumferential velocity distribution of the vortex to the circulation at the tip region of the blade.

$$r = \left|\frac{1}{\Gamma_b(y)}\int_L^y \Gamma_b(s)ds\right| \tag{1}$$

$$v_\theta = \frac{\Gamma_v}{2\pi r} = \frac{\Gamma_b\{y(r)\}}{2\pi r} \tag{2}$$

The unsteady lift on the blade due to blade vortex interaction is calculated using Filotas' linear unsteady aerodynamic theoory. The trailing vortex is approximated as an infinite straight vortex filament and modelled as a series of sinusoidal gusts which interact with an infinite stationary planar wing at an oblique angle. As shown in Figure 5, the vortex filament is located parallel to the plane of the wing, and the induced velocity field at the airfoil location is expressed as

$$w(\xi) = \frac{\Gamma_v}{2\pi} \frac{\xi^2}{\xi^2+h^2} \tag{3}$$

Hence, the effective gust pattern will have a "pseudo" core even though the viscous effect is not accounted for by the vortex roll-up model. If the non-dimensional aerodynamic frequency is defined as

$$\hat{S} = \frac{wb_o}{U} \tag{4}$$

The spectrum of the unsteady lift fluctuation due to BVI is given by Filotas as

$$L_o(\hat{S},\Lambda) = 2\pi\rho U^2 b_o \, T\left(\frac{\hat{S}}{cos\Lambda},\Lambda\right) W(\hat{S}) \tag{5}$$

where the spectrum of the upwash is determined using a discrete Fast Fourier Transform method. The temporal variation of the lift at a spanwise location can be determined via inverse the Fourier Transform. To simplify the acoustic formulation, Widnall models the unsteady lift as a line of acoustic dipoles acting upon an "effective blade-vortex interaction length." The unsteady wave equation is applied with the following boundary conditions,

$$p^-(x,y,o) - p^+(x,y,o) = L\left(t - \frac{x}{U_c}\delta(y - Ut)\right) \qquad |X| \leq S_o \tag{6}$$

$$p^-(x,y,o) - p^+(x,y,o) = 0 \qquad |X| \geq S_o \tag{7}$$

The tip effect is accounted for by an abrupt truncation of the line of dipoles with the use of a delta function. A more detailed account of the theory can be found in reference 3.

DATA REDUCTION PROCEDURES

The sectional lift at the 76 and 99 percent span were obtained by integrating the differential pressure measurements along the chordwise direction. The Kutta condition is imposed by requiring a zero pressure gradient across the rotor disk at the trailing edge. The local circulation is then related to the sectional lift by the Kutta-Joukowski theorem.

$$l = \rho U \Gamma \tag{8}$$

The circulation so obtained was then curve-fitted to an exponential sine function which provided the circulation distribution at the tip.

$$\Gamma = \Gamma_{max}\left(sin\,\frac{y\pi}{2L}\right)^{\gamma} \tag{9}$$

For a NACA 0012 blade with square tip the circulation distribution obtained with the exponential sine function correlates well the measured results of Biggers et al[12]. The resulting circulation distribution was input to the Betz vortex roll-up model to construct the roll-up vortex. The blade/vortex separation distance and interaction angle as shown in Figure 5 were determined from the digitized photographs taken during the smoke visualization session. The theoretical upwash which the blade encountered was constructed using the interaction geometry and vortex structure obtained above. The interaction length is determined using the procedures given in [6], and in this case 15.2 cm is used. The far field acoustic signature was then determined. A block diagram of the computational scheme is shown in Figure 6.

RESULTS AND DISCUSSIONS

Figures 7 and 8 present typical pressure transducer and acoustic data collected simultaneously for the case of an advance ratio of 0.17 and rotational speed of 800 rpm on a two-bladed rotor. This data corresponds to case 1 in Table 1. The pressure transducer data is labeled consistently with Figure 3. The presence of a vortex at the 40 degree azimuth is strongly indicated by a large amplitude fluctuation on the output of the leading edge pressure transducers. An upwash, which causes an increase in angle

of attack and results in higher lift, is evident on the leading edge pressure transducer measurements, followed by a decrease in the differential pressure and subsequent lift. This pressure variation trend is consistent with the orientation of the trailing vortex for an inverted rotor. As shown in Figure 8, an impulsive acoustic signature is recorded by the microphone approximately 4.1 milliseconds after the presence of the vortex has been detected by the leading edge pressure transducers. This delay time is also evident in the cross correlation function determined for the microphone and leading edge pressure transducer at the 99 percent span location and is shown in Figure 9. This suggests that the large and rapid pressure fluctuations which occur at the leading edge during BVI are responsible for the blade slap. It can be seen in the pressure time histories of Figures 7 and 8 that the chordwise pressure fluctuations induced by the vortex are negligible. These measurements are, therefore, consistent with the assumptions of Widnall/Wolf in modelling the fluctuating lift force as a line of acoustic dipoles. The effects of interaction angles on the peak sound pressure level were also studied using the smoke flow visualization technique[4].

At small interaction angles, the propagation speed of the pressure disturbance caused by the vortex can reach supersonic velocity and accumulate to form a strong and effective radiating wave front to generate a larger and more intense acoustic pulse. Conversely, the interactions which occur at large oblique angles will result in a dispersed wave front and are unlikely to generate impulsive noise. The peak blade slap occurs when there is parallel interaction between the vortex filament and the blade[2]. This has been verified by experiments performed by Fontana and Hubbard[4]. The variation of the peak sound pressure level with the interaction angle is summarized in Table 1.

Figure 10 shows a typical plot of the resulting spanwise circulation distribution for the outer 24 percent span of the blade and was used as input to the Betz vortex model. Figure 11 depicts the vortex structure as predicted by this vortex roll-up model. The core is not modelled and is unlikely to provide good correlation with experiments for interactions occurring inside the core region. For the purpose of comparing the predicted sound pressure signal with experimental results, it is necessary to simulate the blade slap condition with BVI occurring just outside the vortex core. The radius of the vortex core for a typical helicopter blade with NACA 0012 airfoil section has been measured to be approximately one-tenth of the blade chord[12]. In all the cases tested, the separation distances as determined by smoke visualization are larger than the

above value and hence, the viscous vortex core is assumed not to contribute significant errors under the operating conditions tested.

A comparison of the predicted and measured waveforms (both are B-Weighted) is shown in Figure 12. The shapes of both pulses are similar, with slight differences in pulse widths. This difference can be explained by referring to the basic formulation of the theory. The peak-to-peak value of the predicted pulse is proportional to the velocity gradient within the core of the upwash, and the width is proportional to the upwash core radius. The structure of the upwash is constructed based on the interaction geometry and the circumferential velocity of the vortex calculated by the Betz vortex model. An increase in the blade vortex separation will result in a smaller and wider upwash pattern. The predicted acoustic pulse will also be wider and smaller. Conversely, a larger and narrower acoustic pulse will be predicted for a smaller separation distance. The vortex core is not modelled in the existing theory. The upwash, constructed on the basis of the interaction geometry, will essentially have a core radius equivalent to the separation distance. The core radius of the upwash constructed using this method will always be smaller than the actual upwash, and will result in a smaller predicted pulse width.

Good correlations are obtained as the advance ratio is decreased to 0.15 and the interaction angle increased to 6 degrees. The measured peak-to-peak sound pressure is 98.1 dB, whereas it is 94.1 dB as predicted by the theory. The effect of the interaction angle on the acoustic pulse are studied theoretically by inputting four different interaction angles to the computer program while keeping the other parameters constant. Figure 13 shows as the interaction angle increases from 0 to 5 degrees, only a slight change in the SPL can be observed. A further increase in interaction angle will cause a rapid decrease of the SPL. Hence, a decrease in peak SPL is consistent with an increase in interaction angle. This is shown both by experiment and theory.

As the advance ratio is increased to 0.19, the interaction angle is decreased to 4 degrees and the separation distance is increased to about 1.8 times of the chord. The theory is expected to provide good correlation in this case as the interaction occurs in the inviscid portion of the upwash. However, the theory fails to show good correlation in this case. It underpredicts the peak-to-peak SPL by about 10 dB. This discrepancy is not due to the vortex model of the theory, but rather it is due to the skew angle effect which was observed by smoke visualization. The blade vortex separation distance in this case varies in the spanwise direction. The effect of the separation distance was

investigated by using four different separation distances in the prediction code, keeping all other parameters constant. As shown in Figures 14, 15 and 16 a slight increase in separation distance will increase the core radius of the upwash and decrease the amplitude significantly. The resultant acoustic pulse is more dispersed and less intense. As illustrated in Figure 17 a 3.5 cm increase in separation distance can can contribute a 5 dB difference in the peak-to-peak SPL prediction. Hence, a modification of the theory is necessary for this particular interaction geometry.

CONCLUSIONS

A unique data acquisition system has been developed to allow a transfer of pressure transducer and hot film data from a rotating frame to a stationary frame. This system also allows for the collection of both loading and far field acoustic measurements simultaneously and makes the comparison of experimental and theoretical predictions of the relation between blade loads and far field acoustic possible. Temporal correlation techniques have been used to determine the cause of blade slap on the advancing side of the rotor disk. The interactions which occur at shallow interaction angle ranging from zero to 6 degrees and the resulting disturbance is, in fact, a very efficient radiating acoustic source. The rapid pressure fluctuations which occur at the leading edge during BVI have shown a good correlation with the associate acoustic impulse and is the most important noise producing mechanism.

The predicted acoustic pulse has been compared with experimental measurements. The assumptions made in the Widnall and Wolf theory have been verified and are shown to be valid at low speed incompressible flow. Good correlations are shown for the BVI which occur at interaction angles less than 6 degrees and at a region outside the vortex core where the viscous effect is insignificant. The peak-to-peak sound pressure levels are predicted to within 4 dB. The width of the acoustic pulse is underpredicted due to the effect of the vortex core which is not modelled by the theory. The theory is also shown to be very sensitive to the interaction geometry, in particular with the separation distance, and the trajectory of the trailing vortex. Poor correlation is shown for the case in which the vortex interacts with the balde in a skew angle.

REFERENCES

1. **Farassat, F.**, Theory of Noise Generating form Moving Bodies with an Application to Helicopter Rotors, *TR R-451, NASA 1975.*

2. **Nakamura, Y.**, Prediction of Blade-Vortex Interaction Noise form Measured Blade Pressure, *Seventh European Rotorcraft and Powered Lift Forum, Gamisch-Partenkirchen, Federal Republic of Germany, September 1981.*

3. **Widnall, S.E.** and **Wolf, T.L.**, Effect of Tip Vortex Structure on Helicopter Noise Due to Blade-Vortex Interaction, *Journal of Aircraft 17(10), October 1980.*

4. **Fontana, R.R.** and **Hubbard, Jr., J.E.**, A Comparison with W{Theory of Peak to Peak Sound Level for a Model Helicopter Rotor Generating Blade Slap at Low Tip Speeds, *Ninth European Rotorcraft and Powered Lift Aircraft Forum, Stresa, Italy, September 1983.*

5. **Hubbard,Jr., J.E.** and **Leighton, K.P.**, A Comparison of Model Helicopter Rotor Primary and Secondary Blade/Vortex Interaction Blade Slap, *Journal of Aircraft, Vol. 21, No. 5, April 1984.*

6. **Chan, D.C.**, A Correlation of Theory and Experiments Using Measured Blade Loads on A Model Helicopter Rotor Generating Blade Slap at Low Tip Speeds, *Master Thesis, Department of Aeronatuics and Astronautics, Massachusetts Institute of Technology, September 1984.*

7. **McFarland, E.R.**, Solution of Plane Cascade Flow Using Improved Surface Sinularity Methods, *TM 81589 NASA, March 1981.*

8. **Betz, A.**, Behavior of Vortex System, *TM 713, NACA 1932.*

9. **Filotas, L.T.**, Theory of Airfoil Response in a Gusty Atmosphere Part I, Aerodynamic Transfer Function, *Report 139, UTIAS University of Toronto, October 1969.*

10. **Donaldson, C., Snedeker, R.S.** and **Sullivan, R.D.**, A Method of Calculating Aircraft Wake Velocity Profiles and Comparison with Full-Scale Experimental Measurements, *AIAA Paper No. 74-39.*

11. **Rossow, V.J.**, On the Inviscid Rolled-Up Structure of Lift-Generated Vortices, *Journal of Aircraft 10(11), November 1973.*

12. **Biggers, J.C., Lee, A., Orloff, K.L.** and **Luebs, A.B.**, Measurements of Helicopter Rotor Tip Vortices, *Thirty-Third Annual National Forum of American Helicopter Society, Washington, D.C., May 1977.*

NOMENCLATURE

b	blade semi-chord
h	vortex and blade separation distance
L	radius of the blade
L_o	unsteady lift fluctuation
l	sectional lift
p	sound pressure
r	radial position of the vortex
s_o	interaction length
SPL	sound pressure level, db re $\sim$ 0.0002 vbar
T	Lift Transfer Function postulated by Filotas
t	time
U	velocity perpendicular to the blade $u = U\infty\sin\psi + y\omega$
U_∞	free stream velocity
U_c	convection velocity along the blade, $u_c = \frac{U}{\tan\Lambda}$
V_θ	circumferential velocity induced by the roll-up vortex
w	upwash induced by the vortex
W	spectrum of the upwash
x,y	spatial coordinates on the blade see Figure 5
δ	delta function
ξ	See Figure 5
σ	frequency of the upwash
ω	rotational speed of the blade
Γ_b	circulation distribution on the blade
Γ_v	circulation distribution of the roll-up vortex
Γ_{max}	circulation at 76% span
Λ	interaction angle see Figure 5
ψ	azimuth angle the interaction occurs
γ	real number

Table 1: Summary of Correlation of Peak to Peak SPL Between Experiment and Theory

Relative Microphone Position : R = 134 cm θ = 61.5°
ψ = 90°

Number of Blade : 2

Radius of Rotor (R) : 0.6 m

Semi-Chord Length of The Blade (b_0) : 25.44 mm

Interaction Length (a_0) : 15.2 cm

μ	ω (rpm)	Λ (degree)	h/b_0	ψ (degree)	p_{neg} (Pa)	p_{sp} (Pa)	TPP (degree)	Measured SPL (dB)	SPL_t (dB)
0.17	800	8	0.25	45.02	98.10	35.55	3.0	92.0	94.30
0.15	800	4	0.25	52.0	96.11	40.26	6.5	90.1	94.17
0.19	800	4	1.70	35.3	100.00	33.27	5.0	87.0	75.4
0.17	1000	8	0.25	46.0	154.10	67.44	0.5	101.6	90.3

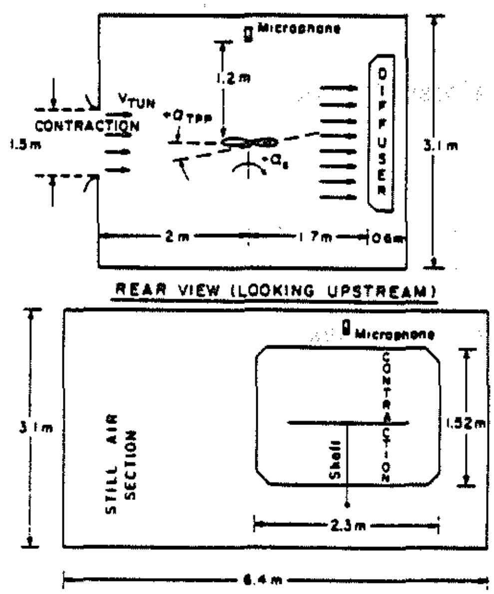

Figure 1: Model Rotor and M.I.T. Anechoic Wind Tunnel

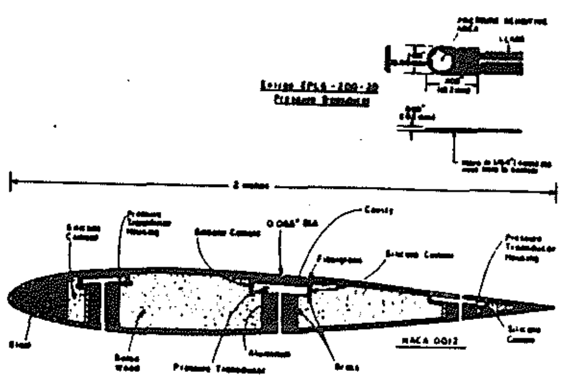

Figure 2: Installation of the Pressure Transducers

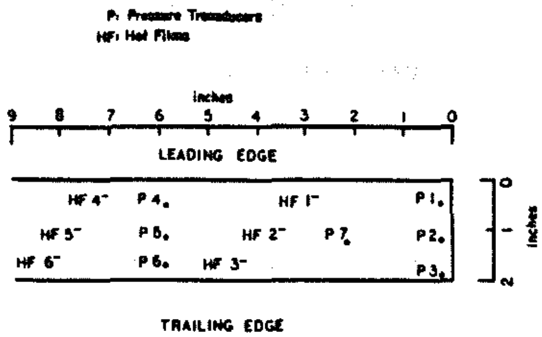

Figure 3: Position of the Pressure Transducers and Hot Films

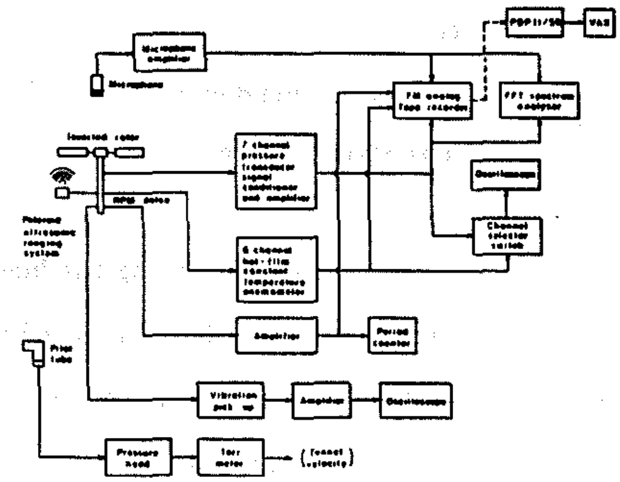

Figure 4: Schematic of the Data Acquisition System

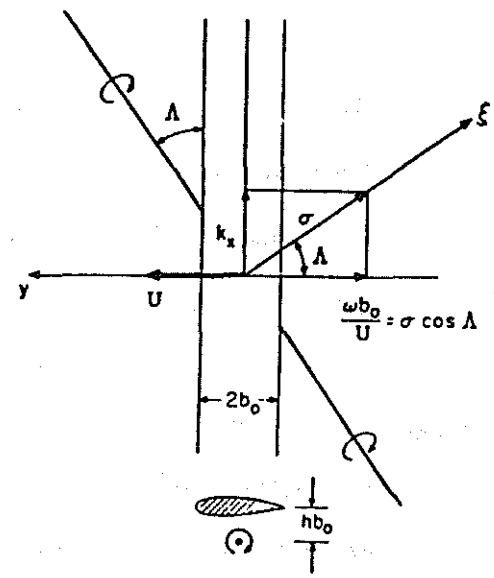

Figure 5: Geometry of Blade/Vortex Interaction
(Note: $c \equiv b_o$ (the blade semichord) for this paper)

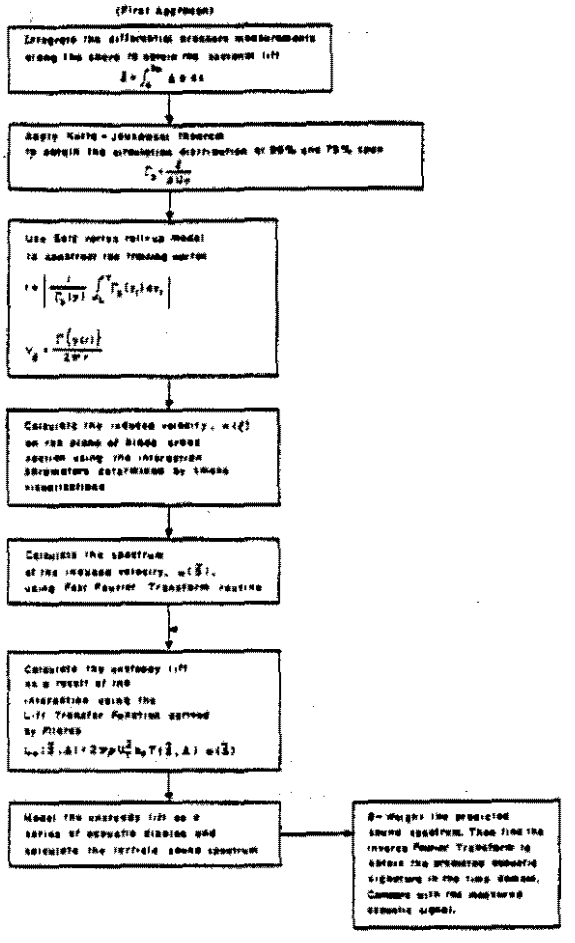

Figure 6: Block Diagram of the Widnall and Wolf Theory

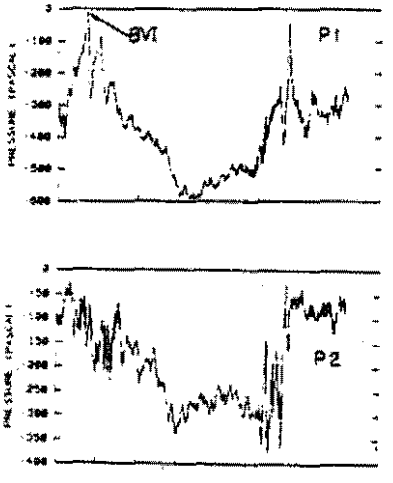

Figure 7: Pressure Measurements for μ=0.17 and ω=800 rpm

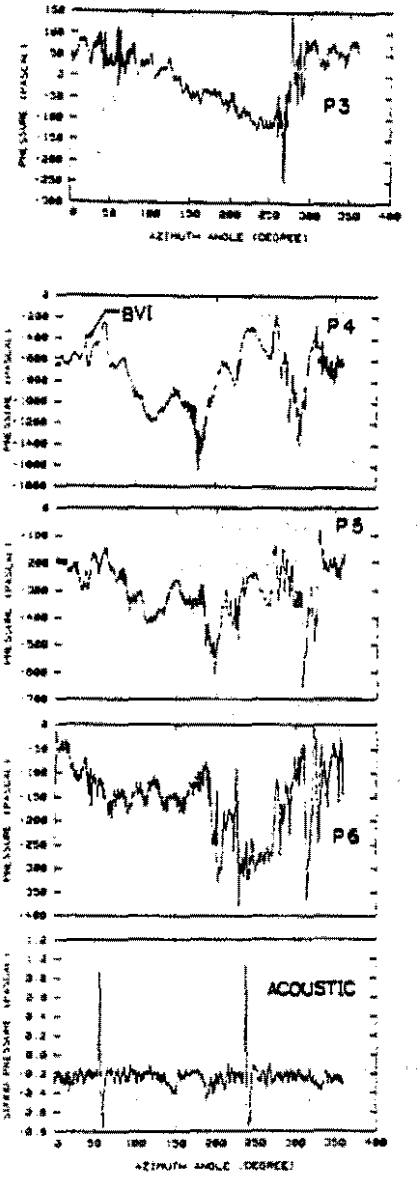

Figure 8: Pressure and Acoustic Measurements for μ=0.17 and ω=800 rpm

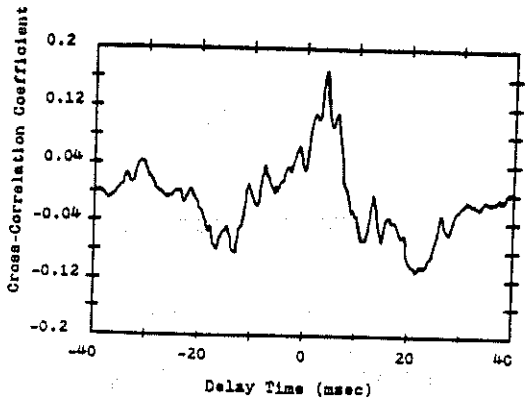

Figure 9: Cross-Correlation Function of the Leading Edge Pressure Measurements and Acoustic Signature

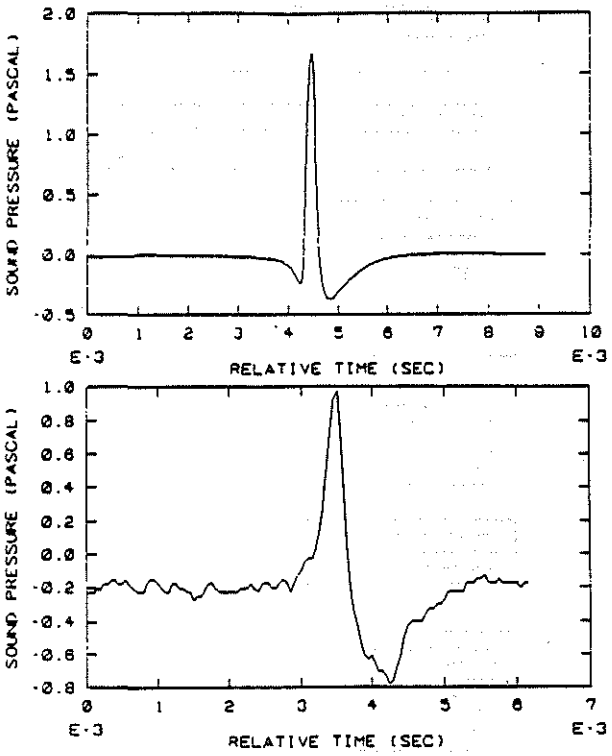

Figure 12: Comparison of the Predicted and Measured BVI Pulse

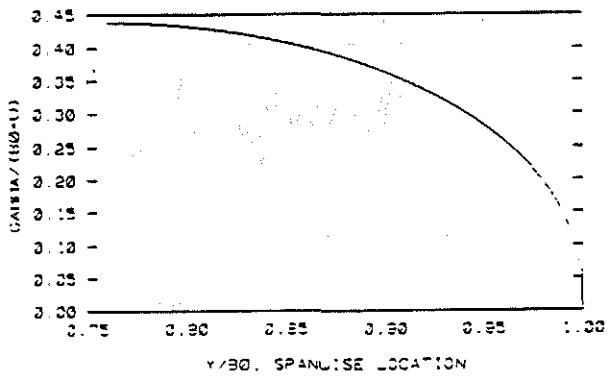

Figure 10: Typical Spanwise Circulation Distribution Determined by this Experiment

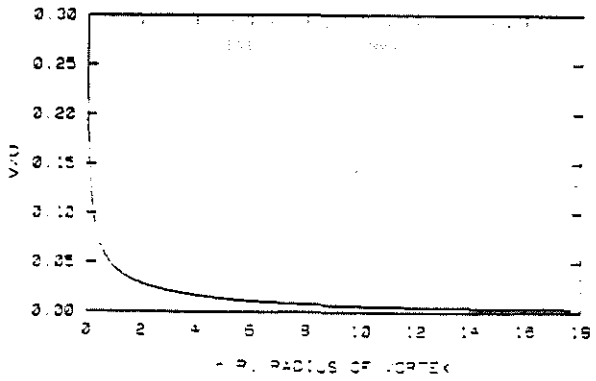

Figure 11: Typical Vortex Structure Predicted by the Betz Model

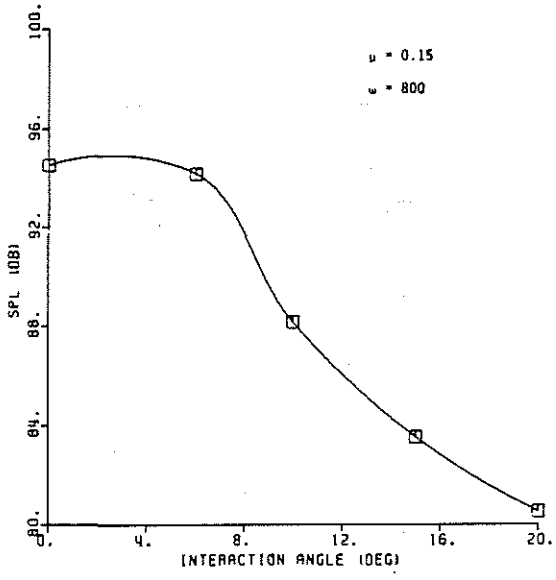

Figure 13: The Effect of Interaction Angle on the Peak SPL

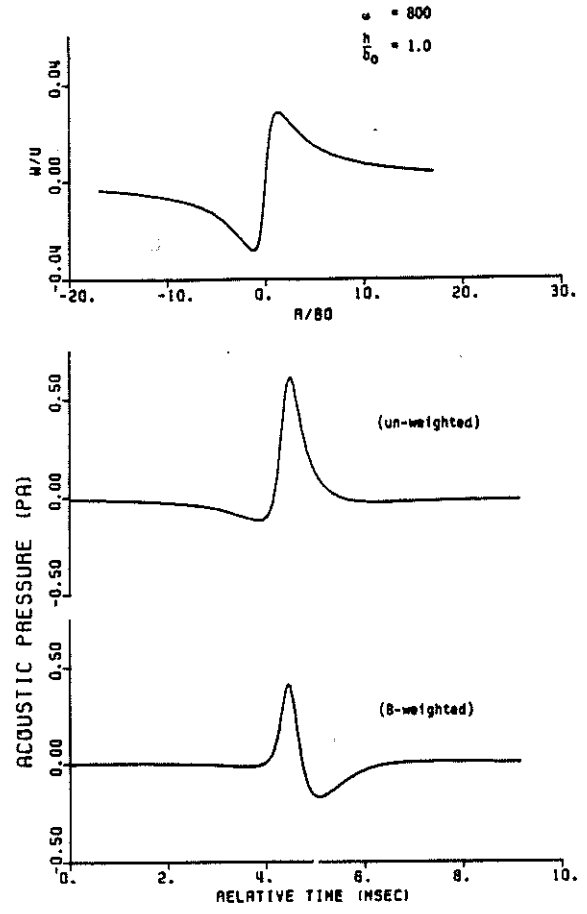

Figure 14: Upwash Pattern and Predicted Acoustic Pulse at $h/b_o = 1.0$

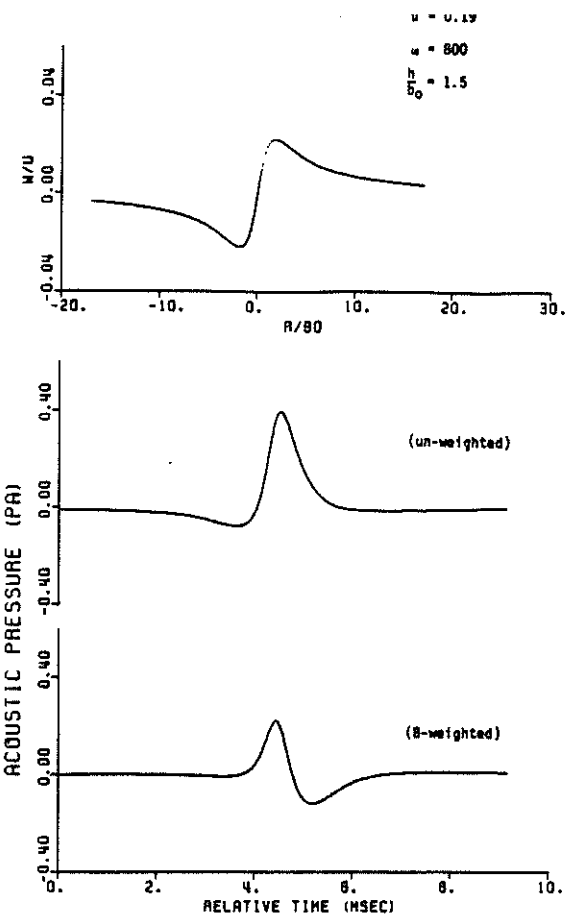

Figure 15: Upwash Pattern and Predicted Acoustic Pulse at $h/b_o = 1.5$

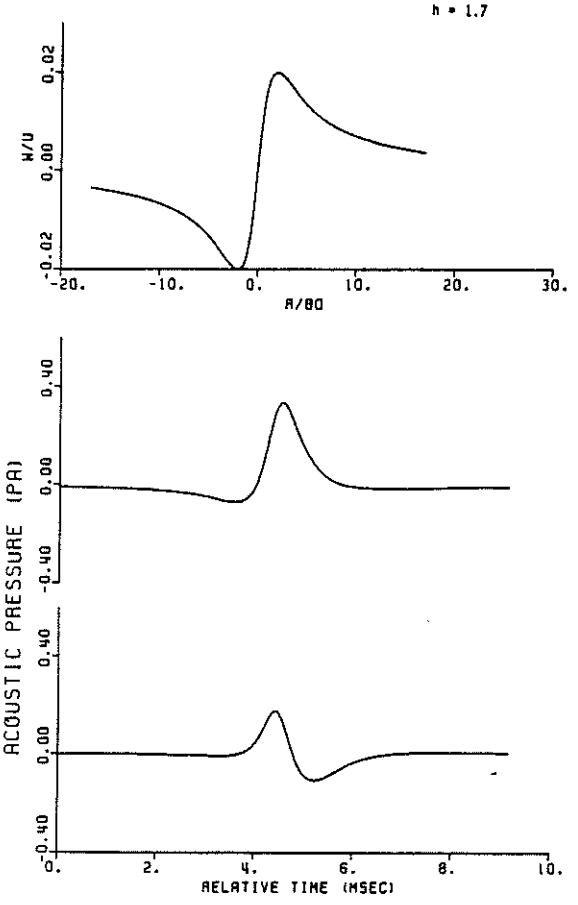

Figure 16: Upwash Pattern and Predicted Acoustic Pulse at $h/b_o = 1.7$

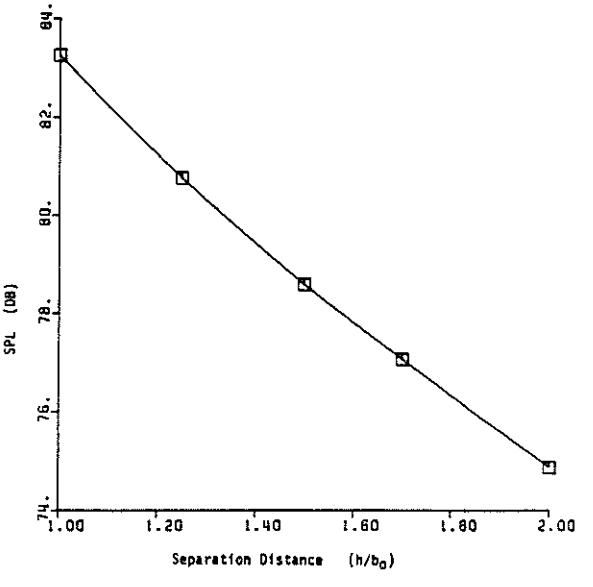

Figure 17: Effect of Separation Distance on the Peak SPL